Sustainable Energy, Grids and Networks 35 (2023) 101128

Contents lists available at ScienceDirect

Sustainable Energy, Grids and Networks

journal homepage: www.elsevier.com/locate/segan

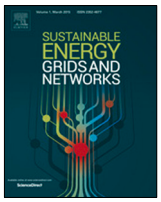

Near real-time analysis of active distribution networks in a Digital Twin framework: A real case study

T. Bragatto [a,*], M.A. Bucarelli [a], F. Carere [a], M. Cresta [b], F.M. Gatta [a], A. Geri [a], M. Maccioni [a], M. Paulucci [b], P. Poursoltan [a], F. Santori [b]

[a] Department of Astronautics, Electrical and Energy Engineering (DIAEE), "Sapienza" University of Rome, Rome, Italy
[b] ASM Terni S.p.A., Terni, Italy

ARTICLE INFO

Article history:
Received 6 December 2022
Received in revised form 13 June 2023
Accepted 26 July 2023
Available online 2 August 2023

Keywords:
Digital Twin
Distribution network
Flexibility
State estimation
Near real-time analysis

ABSTRACT

The growth of distributed generation and the need of increasing Distribution Network (DN) resilience is encouraging Distribution System Operators (DSO) to increase awareness about the real-time status of the network as well as to actively manage flexible energy resources for improving system performances. In this context, Digital Twin (DT) is an enabling technology for a low-cost distributed framework that supports DN management. DT in the power system can be exploited taking advantage of the successful experiences in other sectors (e.g., smart manufacturing and building automation). This article presents a real case study of a DT development and its integration with an existing DN. The DT system architecture is based on the recent standards whilst main DT components have been originally developed, enabling near real-time services such as data collection, state estimation, and flexibility calculator. The individual performances of the integrated tools and the reliability of DT were tested and validated during one month of continuous operation. During the operation, good service continuity and accuracy performances were reported. Results from the flexibility calculator show the effectiveness of the proposed strategies that can improve the energy efficiency of the DN by increasing local self-consumption of Renewable Energy Sources (RES) production.

1. Introduction

In last years, the adoption of Digital Twins in many industrial fields has allowed performing advanced data analytics and the integration of Internet of Things devices. In 2003, Michael Grieves first coined the term "digital twin" [1]; since then, it gained popularity and is now recognized as a key enabler for industry transformation, [2]. According to [3], DT can be defined as "a living model of the physical asset or system, which continually adapts to operational changes based on the collected online data and information, and can forecast the future of the corresponding physical counterpart". A DT can be also defined as a realistic digital representation of built environment assets, processes, or systems [4] that resembles the operation of physical, social, and economic systems and the processes that are articulated alongside and throughout the system's lifecycle [5].

Since the 1990s, DT has been implemented in various industries [6]: applications in manufacturing [7], construction [8], automobile, aerospace, smart manufacturing [7], and electricity [9] are examples of industries that are in the adoption phase of DT [9]. DTs' industrial applications include real-time monitoring, production control, performance prediction, human–robot interaction, optimization, asset management, and production planning. Among DT applications, the main services are predictive maintenance, fault detection and diagnosis, state monitoring, performance prediction, virtual testing [2], diagnosis and adaptive degradation analysis of rotating machines [10], prognostics, and health management [11].

Concerning the power system domain, the DT concept is not widely adopted, as reported in [12] which reviews the most recent trends of DT in microgrids. According to [12], it can be stated that the DT concept is almost mature in some fields; nevertheless, its role in the power system domain is still partially unexplored. In particular, the few papers that address DT in power systems do not exploit the existing standard requirements or the already defined reference architectures for developing a new DT. Indeed, the exploitation of existing standards can be frequently found in other fields whilst, in the power system domain, common approaches are missing and the application borders of DT are wide. In this respect, most recent reviews about DT do not report power systems among application domains of DT; notably, [13] reports manufacturing and precision medicine as the most active application domains, and [14] mentions Smart Cities and Energy as promising application domains. It is expected that DT can be

* Corresponding author.
E-mail address: tommaso.bragatto@uniroma1.it (T. Bragatto).

https://doi.org/10.1016/j.segan.2023.101128

Nomenclature

Acronyms

COM	Component Object Model
DN	Distribution Network
DR	Demand Response
DSO	Distribution System Operator
DT	Digital Twin
EESS	Electrical Energy Storage System
EV	Electric Vehicle
EVCS	Electric Vehicle Charging Stations
GA	Genetic Algorithm
HVAC	Heating, Ventilation and Air Conditioning
OpenDSS	Open Distribution System Simulator
PHM	Prognostics and Health Management
RES	Renewable Energy Source
SCR	Self-Consumption Rate
SMM	Smart Metrology Meter
SMX	Smart Meter Extension
USM	Unbundled Smart Meter

Constants

N_G	Maximum number of generations
N_K	Number of individual in a population
N_N	Number of nodes of the network
N_M	Number of monitored nodes
N_U	Number of unmonitored nodes
P_{max}	Maximum power demand for a flexible load (kW)
P_{min}	Minimum power demand for a flexible load (kW)
E_{max}	Maximum energy shifted in increase (kWh)
E_{min}	Maximum energy shifted in decrease (kWh)
Y_{nj}	Admittance of the branch between node nth and node jth
γ_{nj}	Admittance angle of the branch between node nth and node jth
V_0	Reference voltage of the slack bus of the network (V)
V_{slack}	Voltage of the slack bus (V)

Indices

k	Index for individuals in a population
t_s	Index for time step during State Estimation
g	Index for generation in the GA for state estimation
i	Index for the nodes of the network
t	Index for timestamp
u	Index for genes

Parameters

η_{ch}	Efficiency of the EESS in the charging phase (%)
η_{dch}	Efficiency of the EESS in the discharging phase (%)
P_{idl}	Idling power losses (kW)

Variables

E_t	Energy stored in the storage system at time t (kWh)
F_k	Objective function of individual k
P_n	Active power demand of node n (kW)
P_i^H	Historical active power of the ith node (kW)
$P_{eff}^{ch}(t)$	Power exchanged with the grid at time t during the charging phase (kW)
$P_{eff}^{dch}(t)$	Power exchanged with the grid at time t during the discharging phase (kW)
P_{in}(t)	Power entering in the storage system at time t (kW)
P_{out}(t)	Power leaving in the storage system at time t (kW)
Q_n	Reactive power demand of node n (kVAR)
Q_i^H	Historical reactive power of the ith node (kVAR)
V_i^c	Calculated voltage of the ith node (V)
V_i^m	Measured voltage of the ith node (V)
V_i	Voltage of the ith node (V)
V_n	Voltage of the nth node (V)
$\eta_{inv}(t)$	Percentage efficiency of the inverter at time t (%)
$\phi(t)$	Power variation due to load shifting at time t (kW)
$P_{act}(t)$	Actual power demand at time t (kW)
$E(t)$	Energy shifted at time t due to DR (kWh)
E_i	Energy injected in the main feeder
E_a	Energy absorbed from the main feeder
θ_j	Voltage angle of the ith node (rad)
θ_n	Voltage phase angle of the nth node (rad)

an enabling technology for increasing flexibility exploitation as well as market participation, [15,16]; moreover, it could increase operator awareness and system resilience by leveraging real-time distributed sensors coupled with digital models and relevant applications for actively managing flexibility resources.

However, some examples of DT for individual components of a power system can be found in [17], where a DT is used for monitoring power converters, in [18], which describes DT as a method for automated fault detection with an analytical rotodynamic model, and [19], which implements DT for fault diagnosis and maintenance of power grid equipment and transmission lines. DT was also exploited for increasing awareness about smart grid status in order to increase resilience against cyber-attacks, as in [20,21]. Few works fully exploit the DT concept on an electrical power system; notably, Ref. [22] presents the outcomes of a project where a state estimation was developed for simulation and on-field evaluation by controlling one PV plant for optimized voltage regulation; Ref. [23] reports a DT of distributed energy resources tested in a hardware-in-the-loop environment; finally, in [24] DT is exploited for optimally scheduling an energy storage system.

This paper aims at deploying the DT concept in the electric DNs in an economical and simple way, considering the consolidated architecture and features identified in other fields, such as building management and manufacturing.

At first, the authors surveyed the existing DT architectures that can be used as a reference, mainly exploiting recent reviews on this topic [25]. Once identified the reference architecture, the individual modules of DT were developed.

In this work, the authors developed three separated modules: a data collection module, a state estimator algorithm, and a flexibility calculator. Such modules respectively allow the integration of multiple distributed data sources, the calculation of the power flows (also in case of lack of measurements), and the estimation of the flexibility from Electric Energy Storage Systems (EESS), Electric Vehicle Charging Stations (EVCS) and electrical loads. The modules were developed in order to be integrated in the DT framework as well as to ensure near real-time operation, assuming that field sensors are able to provide near real-time measurements. In this paper, near real-time operation is achieved since the services essentially regard network observability and energy flows optimization. For these services, the frequencies of the updates (e.g., the system status is updated every 3 s) are suitable in order to consider the analysis in near real-time. The whole DT was finally integrated with a real distribution network to validate the modules and evaluate the near real-time performances. Indeed, after the integration, DT continuously worked for a month, then its outcomes were analyzed to finally asses DT validation on a real case study. The paper does not claim to develop modules that are more efficient or accurate than those available in the literature, whilst it reports a real-life integration of the DT and the performance evaluation of the developed modules when integrated into a real network (i.e., data sharing speed, the execution time of the modules and assessment of the impact on Self-Consumption Rate (SCR) thought the flexibility calculator). In particular, the main paper contributions are as follows:

- deployment of a DT based on a consolidated reference architecture [26]
- development of a DT that implements data collection, state estimation, and flexibility calculation of a power DN actuating on a real distribution grid;
- operation of the DT applied to a real case study managing data updating every 3 s;
- performance evaluation of the DT modules, in terms of data sharing speed, execution time of the state estimator considering a month of operation in the field test; assessment of the impact on SCR through the flexibility calculator.

The paper structure is as follows. Section 2 presents the implemented DT architecture, highlights the main DT standards in other fields, and also includes details about the modules. Section 3 presents the real case study where DT is implemented and describes the main characteristics of the DN, the features and the constraints of the installed devices, and the near real-time sensing infrastructure integrated into the DT. Section 4 discusses the results obtained after one month of DT operation and, lastly, Section 5 concludes the paper.

2. DT architecture and modules

2.1. System architecture

A reference architecture is fundamental for DT development, as widely discussed in the last decades [27]. In literature, many papers present DT implementations and their reference architectures, amongst them an interesting classification is provided by [14] which distinguishes:

(a) Unit architecture, a monolithic software architecture for low complexity systems;
(b) System architecture, suitable for a system with several interactions with less complex parts;
(c) System of Systems, with a high number of dependencies in a multi-technology domain.

In the literature, some DT architecture models are proposed and discussed. In [28], the authors show a DT architecture reference model for the cloud-based Cyber Physical System (CPS) to identify various degrees of basic and hybrid computation-interaction modes. Ref. [29] reports an application framework consisting of three main layers (Physical space, Information Processing Layer, and Virtual Layer) and DT is applied on the physical production line of an equipment factory. Regarding power systems, a wide and robust set of architecture models is not available: a review focused on DT for microgrids does not provide any architecture models [12], and a review of DT architectures does not mention any works related to power systems [26]. In [29] a DT architecture in the power system is provided: the DT extends the SCADA functionalities, performing the State Estimation and other additional analysis. In another paper, the power system DT architecture is made of three layers: the physical layer, the edge control system, and the virtual space, in which different modules are implemented [21].

Among the available architectures, this paper takes inspiration from the recent ISO standard for DT in manufacturing [26]. Fig. 1 shows the architecture implemented in this paper. There are two main spaces: on the one hand, the physical entity includes power system equipment (i.e., cables, transformers, loads, and generators), sensors, and actuators; on the other hand, the DT framework comprises the data collection entity, the core entity, and the user entity.

The data collection entity collates all the state changes of the observable elements and sends control programs to those elements when adjustments are needed. This entity contains sensor adapters, data storage, and data pre-processing.

The core entity contains the models of the DT, reads the data collected by the data collection entity, and uses the information to update its models. The core entity includes both services and models and, according to [26], the core entity should be divided into two sub-entities, namely Operation and Management sub-entity and the Application and Services sub-entity. In this work, the authors developed a State Estimation module that exploits a limited set of available measurements and increases awareness about network status. Therefore, this module includes a network model and topology and exploits historical data to forecast the load profiles. Concerning the services, a flexibility calculator was developed and it estimates the orders to be sent to flexibility sources that were previously identified.

Finally, the user entity contains the user interface of the services, namely visualization of the outcomes of the modules and the set points for the flexibility orders.

2.2. Data collection

The Data Collection entity is a fundamental part of the DT architecture since it enables a near real-time operation and continuous interaction with the physical entity. Its role in the DT architecture is shown in Fig. 1 and further details are provided in Fig. 2. The entity encompasses sensor adapters, data storage, and a pre-processing function, and its architecture was not designed to limit the sensors that can be integrated; notably, different open protocols and open data formats can be smoothly integrated into the DT by developing related adapters.

Adapters extract relevant information from the sensor output and collect them. Adapter development is a customized activity that is always necessary because of the wide variety of sensors

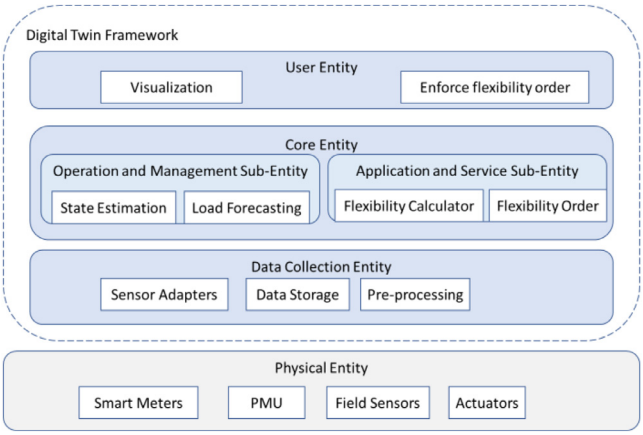

Fig. 1. DT system architecture based on [26].

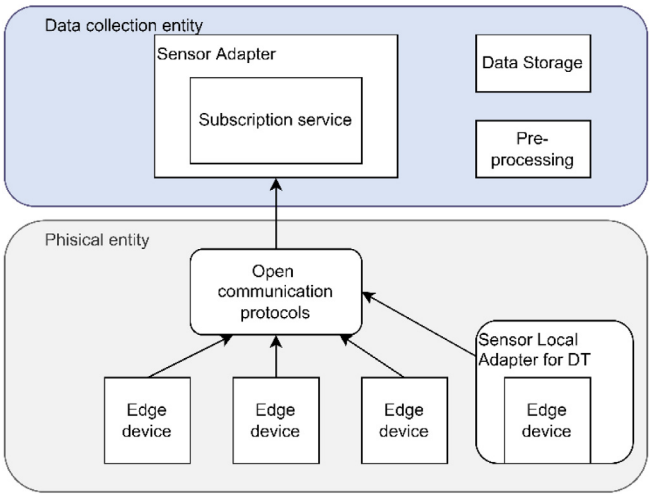

Fig. 2. Data collection entity developed for the case study.

installed in the power systems. Fig. 2 provides insights into the adapters developed in the real case study. In particular, the Data Collection entity takes advantage of existing open protocols as well as edge devices already deployed. An edge device is able to provide measurements even if it is not its main scope, examples are smart meters, power quality analyzers, programmable logic controllers, and smart switch breakers. The added value of the developed central adapter is the adoption of a reference data structure, open and flexible.

2.3. State estimation

The state estimation module was included in the architecture to increase DN observability starting from collected measurements and to provide a digital model of the DN that is further exploited by other modules.

The module receives the actual measurements of the electrical infrastructure as input, namely, voltages and powers at network nodes equipped with smart meters. Measurements are used to calculate power flows along the lines, solving the load flow problem using OpenDSS [30] integrated into the Python environment through the COM interface, the related library is available online [31]. OpenDSS was selected among power flow solvers since it is an open-source product tailored for analyzing DN issues, able to analyze unbalanced networks; moreover, a variety of additional libraries can be coupled with the power flow analysis by interfacing the solver with the Python environment. In particular, OpenDSS calculates node voltages by solving the following system of nonlinear equations:

$$\begin{cases} P_n = \sum_{i=0}^{N_N} V_n V_i Y_{ni} cos(\theta_n - \theta_i - \gamma_{ni}) \\ Q_n = \sum_{i=0}^{N_N} V_n V_i Y_{ni} sin(\theta_n - \theta_i - \gamma_{ni}) \\ V_{slak} = V_0 \end{cases} \quad (1)$$

In (1), P_n and Q_n are active and reactive power at the node n, V_n and θ_n are the node voltage and its phase angle. V_j and θ_j are the voltage and angle of the ith node; N_N is the number of nodes of the network; Y_{nj} is the branch admittance and γ_{nj} its related angle. The system, which is summarized in (1), has (2^*N_N −1) equations (i.e., 2 equations for each node); the remaining node is the slack bus for which the reference voltage V_0 is set.

The power flow calculation in OpenDSS [30] requires the input of the active and reactive power of all nodes as well as the voltage of the slack bus. If the number of monitored buses is not sufficient to solve the power flow problem, the estimation of missing active and reactive power is needed. Voltage measurements are used to verify if the proposed estimation is acceptable according to a predefined tolerance.

In order to estimate the missing power values a GA is used. It calculates the combination of active and reactive power of the unmonitored buses minimizing the error between monitored and calculated voltages. Although State Estimation can be implemented by adopting well-known techniques [32], GA can be useful for state estimation problems when observability requirements are not fulfilled. For this reason, this choice increases the module flexibility when integrated into the DT and applied on different networks. Among the GA versions collected in [33] in the DT a micro-GA is used. In comparison to the other GAs, the micro-GA starts with a smaller random population and converges in a few generations. It was implemented using PyGAD [34], an existing library written in the Python language, using the options for single-point crossover, steady-state parent selection, and random mutation.

The flowchart in Fig. 3 shows the details and functionalities of the state estimation module. After collecting network parameters and topology, these are imported into the OpenDSS input file, which requires to know the value of $2N_N - 1$ electrical variables in order to perform the power flow analysis. When the state estimation starts (i.e., $t_s > 0$), the module considers the measurements that have been just collected and stored. Among these, measured active and reactive power, as well as the voltage of the slack bus are included as input variables in the OpenDSS input file. N_U nodes are the unmonitored nodes, whilst $2N_U$ (i.e., active and reactive power values) are the resulting missing variables that GA has to calculate.

The GA is initialized and parametrized considering actual missing variables, each of them corresponding to a gene (i.e., each individual has $2N_U$ genes). Each gene can vary in a discrete range defined according to historical data. As an example, the structure of the whole chromosome is reported in Table 1; in that case, the range is defined between $0.8P_i^H$ and $1.2P_i^H$. In Table 1, P_i^H is a value that can reasonably approximate the actual value to be estimated by the GA for node i (e.g., the historical measurement of that specific hour and weekday that is under evaluation). This is a weak limitation of the DT since a power value highly different from the historical data is not allowed, but this seems to the authors a good compromise between DT accuracy and execution time.

After the initialization, the sequence of generations starts, as it is reported by the flowchart in Fig. 4. For each generation

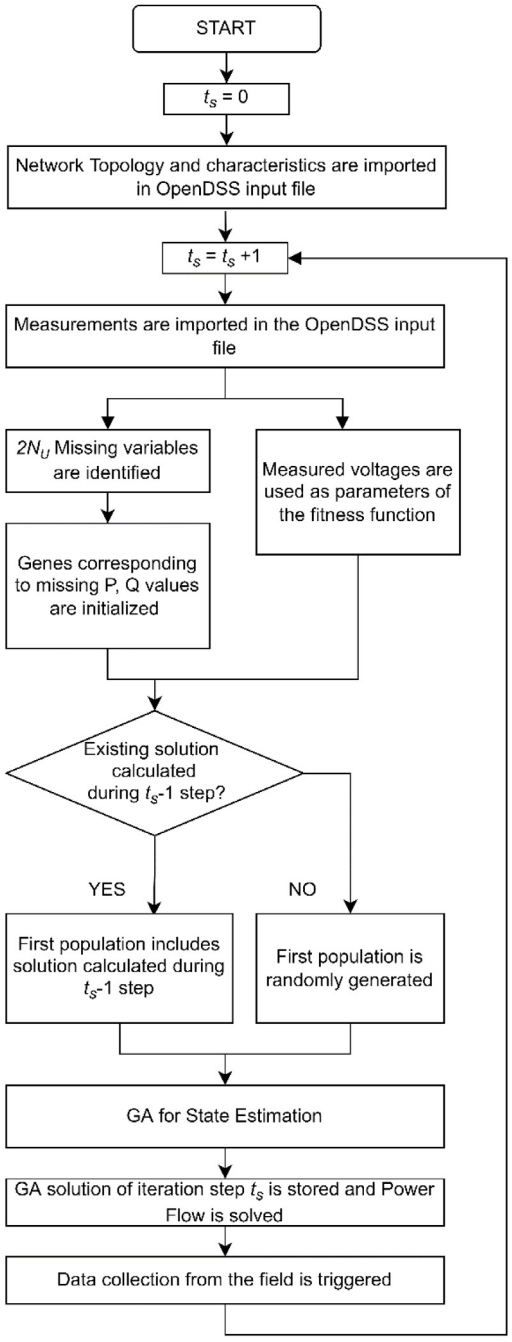

Fig. 3. State estimation module in the DT.

g, GA defines the parameters of all N_K individuals. Then, the fitness of each k individual generated by the GA is calculated by using the genes of the individual to complement the input file to the OpenDSS power flow. In this manner, the estimated values of active and reactive power are included in the power flow calculation. After updating the file, OpenDSS, which is coupled with the GA, calculates power flow and provides a set of voltages that are compared with the measured values. The actual fitness assigned to each k individual is finally calculated according to the following equation:

$$F_k = \frac{N_M}{\sum_{i=1}^{N_M} |V_i^m - V_i^c|} \tag{2}$$

In (2), N_M is the number of monitored nodes for which voltage values are measured, V_i^m and V_i^c are the measured and calculated voltage of the ith node, respectively. Eq. (2) requires in input the measured voltages that are collected in the previous step, according to the flowchart. The best individual is the one with the maximum fitness.

As shown in Fig. 4, two stopping criteria are considered: the tolerance on voltages and the maximum number of generations (i.e., $g = N_G$). As soon as one stopping criterion is achieved, the best individual is stored as the solution of the GA-based state estimation. The solution obtained by the GA complements the OpenDSS input file, and thus the power flow of the network is calculated. The new power flow solution is used by the other modules that perform additional calculations, such as flexibility estimation as explained in the following subsection.

In the first time step $t_s = 1$ the population is randomly initiated, but when $t_s > 1$ the best individual of time step $t_s - 1$ is incorporated in the individuals of the first population. Indeed, as shown in Fig. 3, the GA is continuously invoked by the state estimation tool and if the time interval between two consecutive steps t_s and $t_s + 1$ is small, it makes sense to initialize the state estimation solver with the solution calculated in the previous time stamp. This approach allows to reduce the GA execution time and quickly fulfills the assigned tolerance, making the DT able to operate in near real-time and therefore to be invoked many times per minute. When the solution in the time step $t_s - 1$ is the starting point of step t_s, the GA starts from a solution that already has high fitness, and in a few generations can fulfill the algorithm tolerance. Therefore, even if each GA elaboration can be quite limited, a cycling update of the initial population can easily lead to a solution that fulfills the assigned tolerance.

The complete set of GA parameters used in the case study is included in Table 2.

2.4. Flexibility calculator

The flexibility calculator is a module included in the DT to manage the distributed flexibility resources connected to the DN. According to [35] the flexibility of a component is the ability to change or modify its routine operation for a limited duration, and respond to external service request signals, without inducing unplanned disruptions. This module is in charge of peak shaving and load shifting with the aim of increasing the SCR of renewable sources and of reducing transformers and power lines average and peak load loadings. SCR was implemented as the main objective of the flexibility management since it is relevant for the case study for which the DT is adapted and tested (i.e., the network under evaluation reports some reverse power flow events); nevertheless, other objectives could be considered in the future.

SCR is the ratio of the portion of the RES production consumed by the loads over the produced energy (E_p) of the RES plant. It ranges between 0% and 100% and its expression as a function of energy injected (Ei) is reported in (3).

$$SCR = 1 - \frac{E_i}{E_p} \tag{3}$$

To perform this task, OpenDSS is interfaced with a Python module, exploiting a control strategy of flexibility resources based on the power flow value at the connection with the external network (e.g., the power line or the transformer). Flexibility resources include network elements such as:

- EESS;
- Flexible loads, i.e. Heating, Ventilation and Air Conditioning (HVAC), water pumps, and other time-dependent loads (dishwasher, refrigerator, washing machine) for which a DR mechanism is applied;

Table 1
Structure of the chromosome in GA for state estimation.

Gene Index	1	...	N_u	$N_u + 1$	...	$2N_u$
Values	$[0.8P^H_{1,}, 1.2P^H_1]$	...	$[0.8P^H_{N_u}, 1.2P^H_{N_u}]$	$[0.8Q^H_{1,}, 1.2Q^H_1]$	...	$[0.8Q^H_{N_u}, 1.2Q^H_{N_u}]$

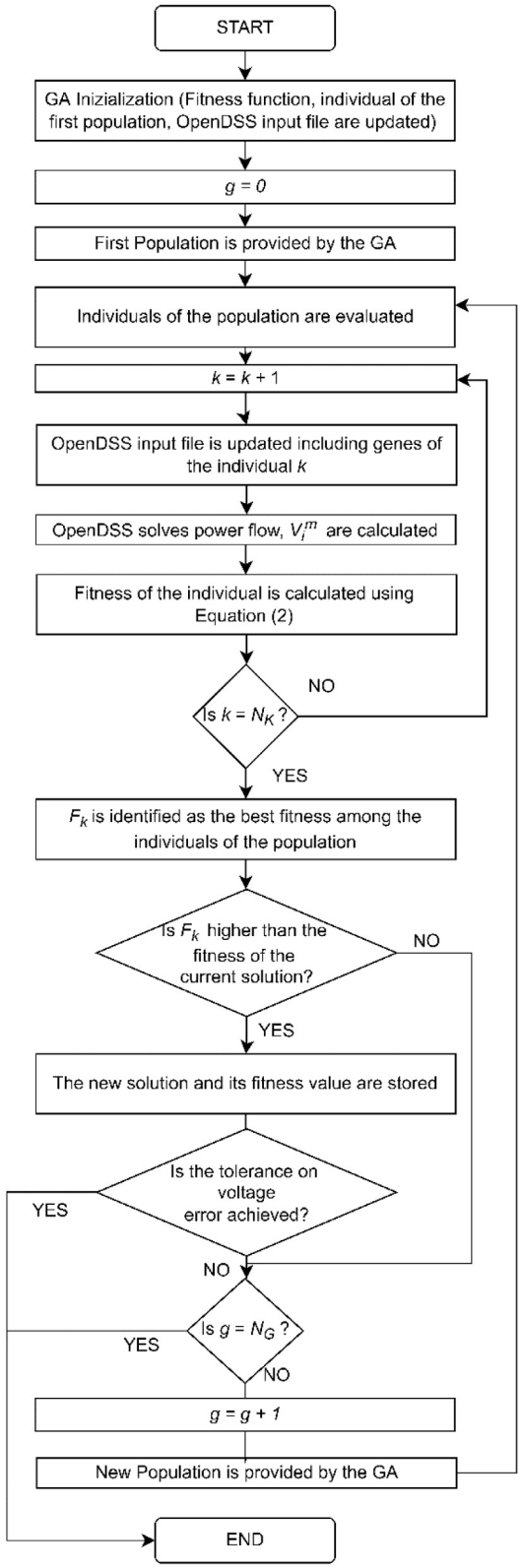

Fig. 4. GA for state estimation.

Table 2
GA parameters for the case study.

Population	5
Maximum number of generations	50
Absolute tolerance on average error	0.25 V
Percentage of genes to mutate	10%
Number of parents to keep in the population	1
Number of solutions to be selected as parents	4
Type of crossover	Single-point
Parent selection type	Steady-state selection
Type of the mutation operation	Random

Table 3
Storage object main features.

State	Storage state: 1) Idling, 2) charging, 3) discharging
% Discharge	Discharge rate in percent of the nominal power (%)
% Charge	Charging rate in percent of the nominal power (%)
η_{ch}	Charging efficiency (%)
η_{dch}	Discharging efficiency (%)
$E(t)$	Available energy at time t (kWh)
$P^{ch}_{eff}(t)$	Power charging the storage at time t (kW)
$P^{dch}_{eff}(t)$	Power discharging the storage at time t (kW)
$P_{in}(t)$	Power injected in the storage by the grid at time t (kW)
$P_{out}(t)$	Power injected in the grid by the storage at time t (kW)
P_{idl}	Idling power losses (kW)

- EVCS.

The flexibility resources have different features, such as the ability to exchange power with the grid in one-way or two-ways, the nominal power, the capacity, and the operating hours. For example, some devices can be activated only for a limited duration service, while other devices can operate for many hours per day. In the following, each flexibility resource model is described.

2.4.1. Electrical energy storage system

In OpenDSS, the storage system object is a power conversion element modeled as a constant power load during the charging phase and as a generator during the discharging phase. An EESS is always constrained by its nominal power and by the stored energy. As shown in Fig. 5, the model consists of a storage element that varies its state of charge during operation, and an inverter that allows dispatching the desired amount of reactive power according to a selected power factor. The main features of the storage object are reported in Table 3.

When charging, the following balance equation applies:

$$E(t + \Delta t) = E(t) + P^{ch}_{eff}(t) \cdot \Delta t \tag{4}$$

being

$$P^{ch}_{eff}(t) = (P_{in}(t) \cdot \eta_{inv}(t) - P_{idl}) \cdot \eta_{ch} \tag{5}$$

When discharging, the balance equation is:

$$E(t + \Delta t) = E(t) - P^{dch}_{eff}(t) \cdot \Delta t \tag{6}$$

being

$$P^{dch}_{eff}(t) = \frac{P_{out}(t)}{\eta_{inv}(t) \cdot \eta_{dch}} + \frac{P_{idl}(t)}{\eta_{dch}} \tag{7}$$

In addition, constraints related to maximum and minimum state of charge, injected/absorbed power and voltage are applied.

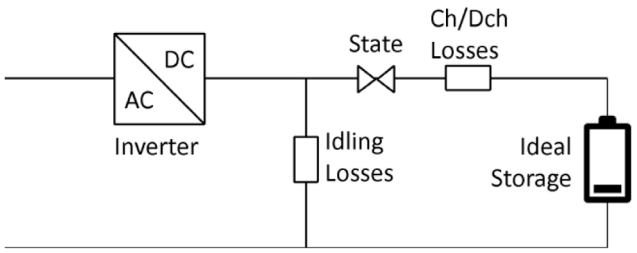

Fig. 5. Storage model.

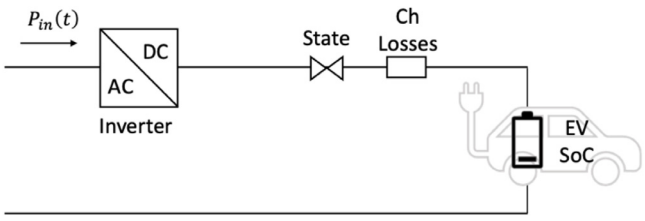

Fig. 6. EVCS model.

Table 4
EVCS model main features.

State	1) Charging, 2) Discharging
% Charge	Charging rate in percent on the nominal power (%)
η_{ch}	Charging efficiency (%)
$SOC_{EV}(t)$	State of charge of the EV connected to the EVCS at time t (%)
$En_{EV}(t)$	Nominal capacity of the battery of the EV (kWh)
$P^{ch}_{eff}(t)$	Power charging the EV at time t (kW)
$P_{in}(t)$	Power injected in the EV by the grid at time t (kW)

When the storage element is idling, the idling losses and the associated inverter losses are supplied by the grid so that the state of charge of the storage does not change.

2.4.2. Electric vehicle charging station

Recent advances in smart grids enable the active and passive participation of EVs in the grid, both individually and in aggregate. The ability of an EVCS to control power flow allows them to exploit their full potential within the electricity DN by providing ancillary services.

In this paper, as also observed in various literature sources [36], EVCSs are simulated with a behavior similar to that of storage systems, limiting the mode of operation to charging only. Table 4 reports the main features of an EVCS as modeled in this paper.

Only grid-to-vehicle was considered, whereby the power supply is reduced according to the needs of the grid, thus only allowing operation when charging vehicles. The EVCS is enabled as a source of flexibility only when, by reading the results obtained by the state estimation, it appears that a vehicle is charging; the power that can be shifted in time covers a percentage between 25% and 100% of the rated power of the EVCS. No user engagement criteria are considered, but it is possible not to enable EVCS for flexibility if the user needs charging at maximum power, without providing an auxiliary service to the network.

When charging, the following balance equation applies:

$$SOC_{EV}(t+\Delta t) = SOC_{EV}(t) + 100 \cdot \frac{P^{ch}_{eff}(t) \cdot \Delta t}{En_{EV}(t)} \tag{8}$$

being

$$P^{ch}_{eff}(t) = (P_{in}(t) \cdot \eta_{inv}(t)) \cdot \eta_{ch} \tag{9}$$

In addition, constraints related to the maximum state of charge, absorbed power, and voltage are applied. When there are no EVs connected to the EVCS or the EV is fully charged, power losses are nil.

Fig. 6 reports the simplified model of the EVCSs.

2.4.3. Flexible load for DR

DR refers to variations in electricity use by end-user loads compared to their typical consumption patterns, in response to changes in electricity prices or incentive payments designed to induce lower electricity use during periods of high wholesale market prices or when system reliability is put at risk.

DR can be triggered with two main processes: self-dispatch participation, i.e., price-based DR where consumers carry out load shifting in order to save economically as a response to price signals; incentive-based DR, where consumers are provided with a benefit (often economic) if they can provide a certain load reduction or load increase over a certain period of time, according to the needs of the electricity grid.

There are numerous DR models in the literature with varying degrees of complexity, taking into account or not the internal characteristics of the equipment as well as technological, social, and environmental factors. In this paper, the authors chose to use an aggregate, simplified type of model that realizes DR by load shifting [36–39].

Load shifting is the most common type of DR. Loads that can be shifted are typically thermal loads (air conditioning, heating, cooling), deferrable loads (washing, ventilation, water pumps), or physical storage systems (hydrogen production). Load shifting is subject to technical constraints, e.g., lack of automation in electric devices or no possibility of load curtailment, user behavioral constraints, process requirements (e.g., some processes cannot be interrupted or modified once started), and availability of appliances, as in [40].

The model of load shifting used for the DT is similar to the ones of storage and EVCSs, i.e., it is as if the flexible load can "produce" power by not consuming it at specific times, and can "consume" power at other times by increasing the base or expected demand curve. The model used in the DT is a DR with load shifting including saturation without a base demand profile [41]; when charging, the following balance equations apply:

$$P_{DR}(t) = P_{act}(t) + \phi(t) \quad \forall t \tag{10}$$

$$\sum_{t=1}^{T} \phi(t) = 0 \tag{11}$$

$$P_{min} \le \phi(t) + P_{act}(t) \le P_{max} \quad \forall t \tag{12}$$

$$P_{DR}(t) \ge 0 \quad \forall t \tag{13}$$

$$E(t) = E(t-\Delta t) + \phi(t) \cdot \Delta t \quad \forall t \tag{14}$$

$$E_{min} \le E(t) \le E_{max} \quad \forall t \tag{15}$$

$$E(t=T) = E(t=0) \tag{16}$$

Eqs. (10)–(13) are the constraints of an ideal shifting of power without a base demand value, where $\phi(t)$ is the power variation due to the DR mechanism in a certain time period. P_{min} and P_{max} depend directly on the type of load in which the DR mechanism is to be realized. To not change the overall consumption, (11) imposes that increments and reductions are balanced over the time span T. Eqs. (14)–(16) involve the free variable $E(t)$ which represents the energy displaced over time by the mechanism, i.e., the capability to anticipate or postpone the consumption, in analogy to EVCS and EESS. In particular, (15) models the load saturation effect by imposing a minimum and maximum level

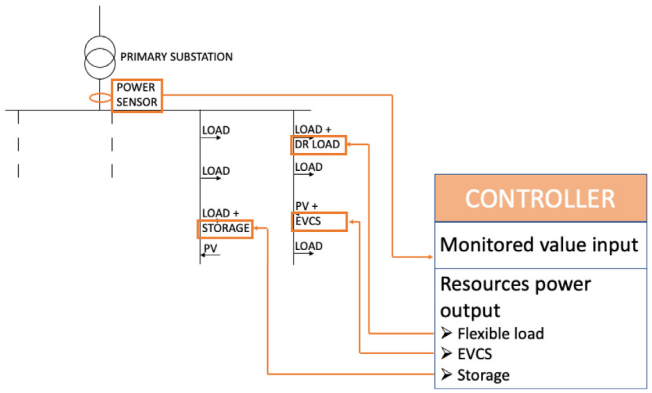

Fig. 7. Storage controller mechanism.

of storage capacity: in this way, unlimited load overconsumption (over-curtailment) during many consecutive periods is not allowed, because the storage will reach its maximum (minimum) level. Eq. (16) ensures that the storage level returns to its initial value at the end of the time span T, thus guaranteeing that load demand can be shifted, but the total overall energy consumption will remain the same.

2.4.4. Flexibility resources management

To manage the behavior of the flexible resources, an operation criterion must be provided, which may be internal to the flexibility resource object or, as in most cases, a controller object may be used. OpenDSS has some pre-set modes for controllers, based on power flow or time-scheduling, but the authors decided to implement a self-written controller in Python using the py-dss-interface module, which allows for varying of the operating state and the power absorbed or injected by the flexibility resource. Each resource can have a different controller or a controller can manage more devices, as in the DT proposed in this paper and described in Fig. 7.

The controller's model written by the authors was developed within Python and interacts with OpenDSS via the COM Interface. It is based on the value measured in the connection element of the network portion with the rest of the network. Based on the value of power flowing against pre-set threshold values, the resource is asked to behave differently, varying the state and varying the amount of power injected or absorbed. The control system acts by detecting the power flowing in the main feeder and in the following timestamp leads to a withdrawal or an injection of power by the flexibility resources as shown in Table 5. For large power values flowing in the main feeder, the storage injects power and the other flexibility resources avoid withdrawals, while for low power values, the storage recharges and the other flexibility resources increase their consumption.

As written by the authors in the introduction, each developed module does not aim to overcome the state of the art and it has some limitations; indeed, the operation mode of the flexibility resources is the result of a simplification and it is not without flaws since it can rarely cause system stability issues.

To maximize the self-consumption of the network, thresholds were set through a GA. The process works based on all the historical data resulting from the state estimator concerning the power demand and generation, and then using the GA an analysis is carried out for the past period to see which would have been the best choice of threshold values; the vector containing the threshold values is also used for all subsequent iterations until the analysis is stopped. This GA-based optimization was developed using the Python-based open-access library PyGAD [34]. This

Table 5
Storage controller criteria.

Threshold	Flexibility resource status	% charging	% discharge
$P \leq P_{th}^{1}$	Charging	100%	–
$P_{th}^{1} < P \leq P_{th}^{2}$	Charging	75%	–
$P_{th}^{2} < P \leq P_{th}^{3}$	Charging	50%	–
$P_{th}^{3} < P \leq P_{th}^{4}$	Charging	25%	–
$P_{th}^{4} < P \leq P_{th}^{5}$	Idling	–	–
$P_{th}^{5} < P \leq P_{th}^{6}$	Discharging	–	25%
$P_{th}^{6} < P \leq P_{th}^{7}$	Discharging	–	50%
$P_{th}^{7} < P \leq P_{th}^{8}$	Discharging	–	75%
$P > P_{th}^{8}$	Discharging	–	100%

activity is performed using 5 solutions per population for 100 generations, each solution consisting of 8 genes. The algorithm takes 46 min if launched considering one month of data sampled every 20 s. This not negligible execution time has no impact on the DT because it only runs once, whereas the DT is running near real-time. Summarizing, flexibility resources management is carried out in the following steps:

1. Identify suitable resources that can be used (e.g., EVCSs are included only if an EV is charging, some resources can be out of service for maintenance activities, etc.);
2. Management of the flexibility resource depending on the power flow in the main feeder (or the connection with the external network compared to threshold values);
3. The power flow of the network with the device thus configured is solved;
4. The energy stored in each device is updated by (4), (6), (8), and (14);
5. Voltage, current, power, and state of charge values obtained by the use of flexible resources are exported.

Execution time for the above-described five steps is about 0.01 s, ensuring near real-time operation. The operations performed by the flexibility mechanism in each iteration are shown in Fig. 8.

3. Case study

3.1. Case study overview

The case study is conducted in a portion of the medium voltage (MV) distribution system of the city of Terni (in the center of Italy). The distribution system supplies 65,000 customers by means of about 700 secondary substations, for an overall yearly load demand of 390 GWh. Most relevant features are presented in [42].

In the last decade, the local DSO (named TDE, the acronym for Terni Distribuzione Elettrica) has made progress in digitizing the electricity distribution system. TDE has deployed an Advanced Metering Infrastructure for all the customers and has installed a SCADA system for the DN to increase the number of remotely observed and controlled elements. Power quality analyzers, phasor measurement units, and smart meters have been widely installed in the network with the aim of providing near real-time measurements, as described in [43,44]. Finally, the integration of some flexible resources with the grid has been demonstrated in the TDE infrastructure [45,46].

The network section selected for the case study well represents the set of recently installed technologies enabling the DT implementation. The section is an MV feeder that supplies 5 secondary substations, as shown in Fig. 9. Two secondary substations supply the DSO's headquarters, that act as a living lab. Summing up, they comprise 2 PV arrays (185 kWp and 60 kWp rated power,

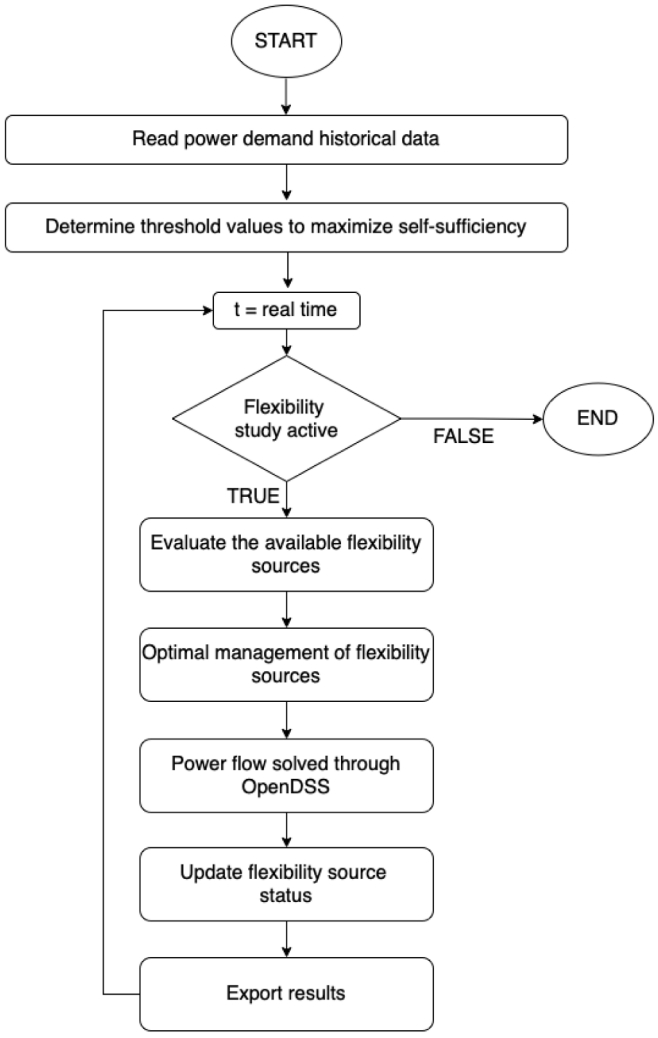

Fig. 8. Flowchart of the flexibility resources management implemented in the DT.

respectively); an EESS equipped with 72 kWh 2nd life Li-ion battery, already presented in [46]; two buildings (6800 m^2) and a 1300 m^2 warehouse. The base load is between 50 and 90 kW, whereas the peak load is between 120 and 170 kW. The HVAC of the building is equipped with a Building Energy Management System; 2 private EVCSs and one public EVCS are installed. A more detailed description of TDE headquarters is presented in [47], whereas Fig. 10 shows some equipment installed in the case study. Moreover, other users are also supplied by the MV feeder, i.e. 1 MV customer and 35 LV customers with an average 400 kWh daily load demand. Some recorded load profiles are plotted in Fig. 11 as an example.

3.2. Monitoring infrastructure and DT integration

The DN of the city of Terni is already partially equipped with a near real-time metering infrastructure. Concerning the physical sensors, the near real-time infrastructure comprises power quality analyzers embedded in the network and smart meters that communicate to a local extension (i.e., a Raspberry pi or another single board computer) which enable near real-time data communication. Further details about this extension developed in previous projects are available in [45,48,49].

Data are put at the disposal of the modules by means of an open protocol (MQTT); smart meters extensions and power

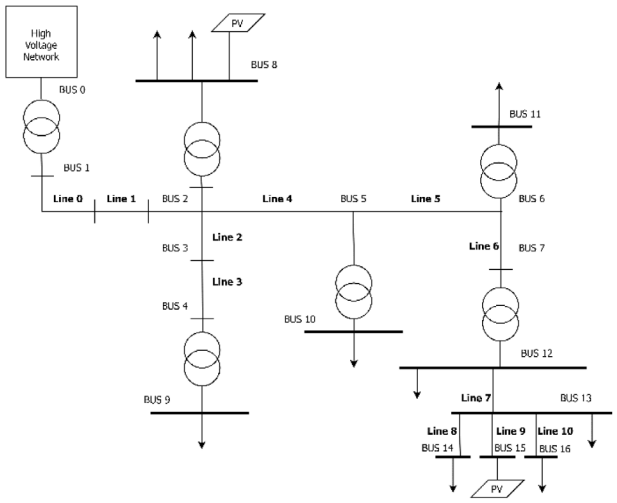

Fig. 9. Single-line diagram of the case study.

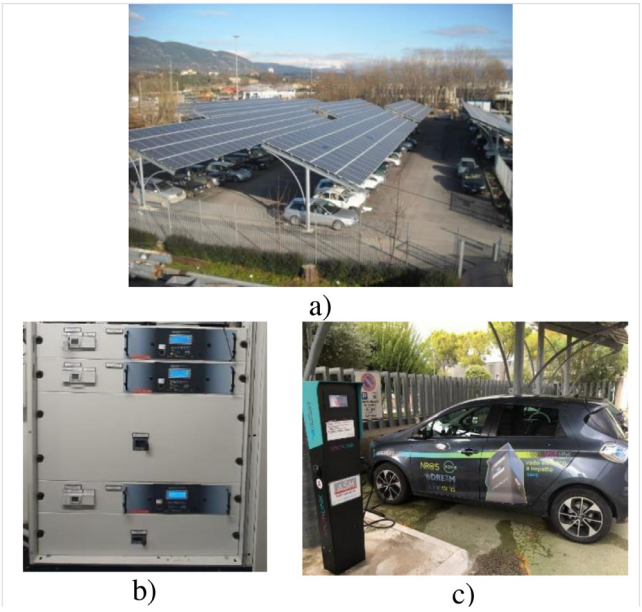

Fig. 10. Some of the equipment installed in the case study: (a) PV plant; (b) metering devices; (c) EVCS.

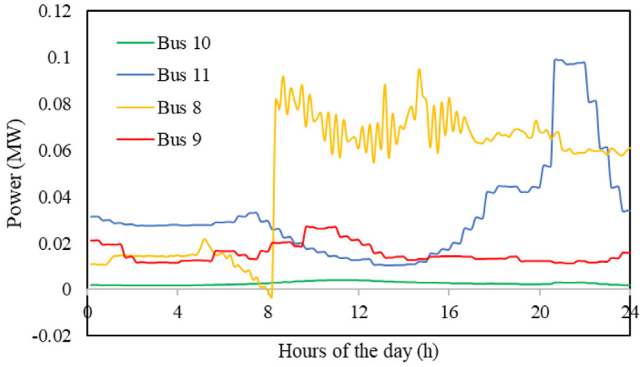

Fig. 11. Example load profiles at some buses of the case study, measured in June 2022.

Table 6
Flexibility parameters for the case study.

Node	Flexibility resources	P_n (kW)	E_n (kWh)
Bus8	DR for HVAC	10	30
Bus11	DR for flexible load	10	10
Bus10	DR for flexible load	5	5
Bus9	EESS	16	16
Bus14	EESS	72	66
Bus8	EVCS	22	70
Bus16	EVCS	50	70

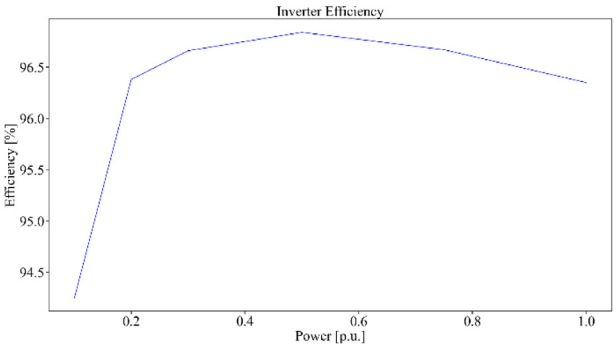

Fig. 12. Inverter efficiency curve implemented in the module.

quality analyzers are configured in order to publish data every second. In order to collect measurements and integrate the smart meters, adapters were developed to subscribe to the relevant topics published by the meters connected in the DN previously described. With respect to the case study, only power quality analyzers are connected to the DN, nevertheless, the developed adapters are suitable even for the smart meters since the data format is the same.

The whole DT of the MV network section was implemented in a remote Workstation with an Intel Core i7-7820X 3.6 GHz CPU and a 64-GB RAM.

3.3. Flexibility resources

Various sources of flexibility are installed in the case study, such as EESS, EVCSs, and flexible loads (through DR). These components are modeled as described in Section 2.4 and their main features are reported in Table 6.

Two typologies of flexible loads are considered, electrical loads to supply HVAC and other loads that can be shifted over time, such as washing machines, dishwashers, and other household appliances. For electrical loads connected to heat consumers such as HVAC, the authors considered that the power that can be shifted over time is 15% of the average power and can be shifted for 3 h over time. For other flexible electrical loads, it is assumed that it is possible to displace 100% of the rated power of the load with an equivalent time of 1 h.

All storage systems are considered to have a unitary power factor. The efficiency curve of the inverter connected to the storage system as a function of the utilization factor is extracted from [45] and plotted in Fig. 12.

As shown in Fig. 7, the management of the resources is based on a unique controller that monitors the power flow in the main feeder, and supplies or absorbs power to maximize the SCR of the grid section. If the positive flow (i.e., from the HV network) is greater than a certain threshold value, the control system requires the flexibility resources to discharge power in order to reduce the upstream power flows and the related network losses. Conversely, if the power flow is lower than a certain threshold value, flexibility resources are requested to charge power in order to reduce/cancel the reverse power flow.

The threshold values used by the controller are updated each time the simulation is launched and, as an example, the threshold values after one month of simulation with a time resolution of 20 s are shown in Table 7. As already explained in the previous section, this calculation does not have an impact on the near real-time operation since it is performed offline.

Due to the small number of flexibility resources available in the case study in comparison with the load, some resources are saturated quickly and the shift of the power flow curve is limited.

3.4. Test network

In order to test the state estimation module in a larger distribution network, additional simulations were carried out applying state estimation on a test network during one day of operation. The tests were carried out on the 33-nodes IEEE test network [50]; 32 nodes are secondary substations with passive loads; the last node is the primary substation. Daily load profiles are simulated considering the base power of each secondary substation and the standard profile based on Ref. [51]. The profile is expressed in p.u. of the peak load and is hourly sampled: spline interpolation is thus applied in order to create load profiles sampled every 20 s; moreover, a random noise is added to differentiate profiles for each substation. Fig. 13 reports the maximum and minimum variation enforced every 20 s: it can be noted that absolute variation does not overcome 20% of the reference profile. The base voltage of the network is 11 kV.

The tests, whose results are presented in Section 4, are focused on the state estimation module since it is necessary to verify that state estimation is properly computed even with a higher number of variables to be managed on a larger network (i.e., the power flow calculation complexity is slightly increased in comparison with the real case study previously presented). Additional tests about the flexibility calculator were not carried out since the thresholds are not updated during the operation; namely, the execution time of the threshold calculation does not impact the operation.

4. Results

4.1. State estimation

During about one month of operation, from 05/08/2022 to 09/09/2022, State Estimation was executed almost 150,000 times (i.e., 3 times per minute): the average execution time was 0.155 s. Anomalous execution times (i.e., higher than 4 s) only occurred 0.1% of the time. The average difference between measured and calculated bus voltages was often acceptable, being 0.024 V, 0.063 V, and 0.140 V in the 1st, 2nd and 3rd quartiles, respectively. Average errors higher than the GA tolerance (i.e., 0.25 V according to Table 1) only occurred 6% of the time.

A detail of state estimation performances is shown in Fig. 14, which reports the average absolute error between state estimation results and measurements (orange line), as well as execution times (blue line) during 75 min operation (in the selected time interval, state estimation has been executed 235 times). Concerning the voltage errors, during 75 min of DT operation the average value is 0.2 V, with a 0.11 V median value. The median value of the execution time of the GA before reaching one stopping criteria is 0.087 s, whilst the average value is 0.46 s. Fig. 14 reports many peaks in the execution time that lead to a higher average value; significant differences among peaks are due to the algorithm that requires fewer iterations before achieving the required tolerance. According to the reported results, it can be stated that

Table 7
Example of the threshold values.

Threshold of the power in the main feeder	Actual value in the case study	Flexibility resource status	% charging/discharging
$P \leq P_{th}^1$	$P_{th}^1 = -12$ kW	Charging	100%
$P_{th}^1 < P \leq P_{th}^2$	$P_{th}^2 = 13$ kW	Charging	75%
$P_{th}^2 < P \leq P_{th}^3$	$P_{th}^3 = 41$ kW	Charging	50%
$P_{th}^3 < P \leq P_{th}^4$	$P_{th}^4 = 53$ kW	Charging	25%
$P_{th}^4 < P \leq P_{th}^5$	$P_{th}^5 = 120$ kW	Idling	–
$P_{th}^5 < P \leq P_{th}^6$	$P_{th}^6 = 164$ kW	Discharging	25%
$P_{th}^6 < P \leq P_{th}^7$	$P_{th}^7 = 172$ kW	Discharging	50%
$P_{th}^7 < P \leq P_{th}^8$	$P_{th}^8 = 265$ kW	Discharging	75%
$P > P_{th}^8$		Discharging	100%

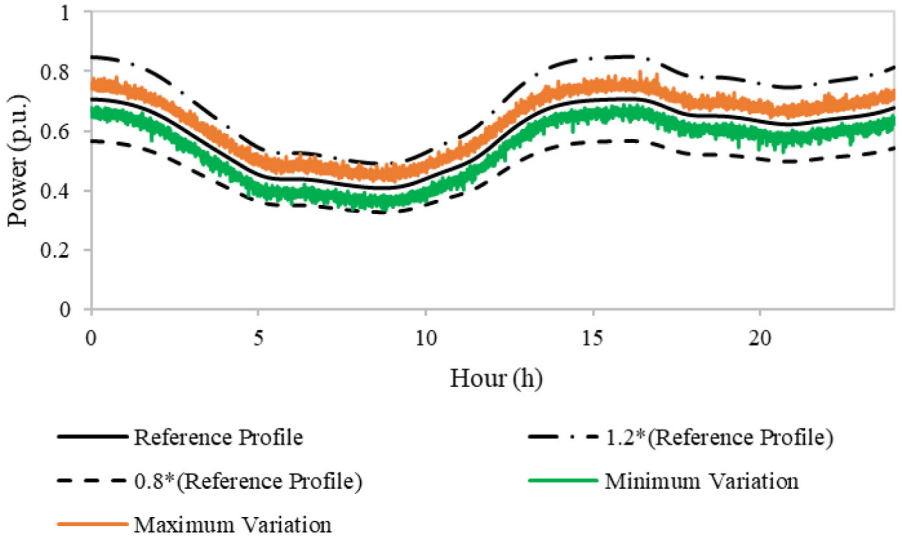

Fig. 13. Reference power profiles and extreme variations evaluated for all timestamps.

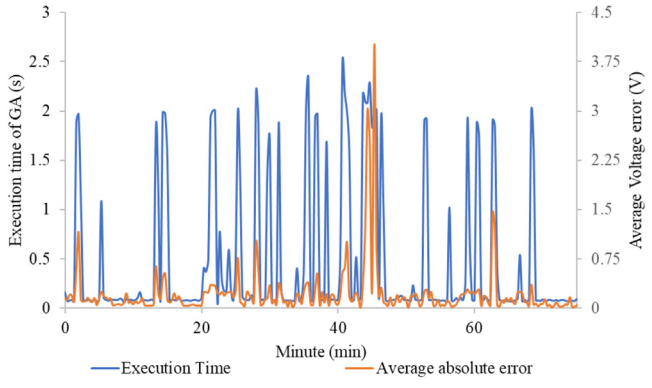

Fig. 14. Execution time of the GA-based state estimation (blue line) and average absolute error between state estimation results and measurements (orange line) during 75 min of operation. . (For interpretation of the references to color in this figure legend, the reader is referred to the web version of this article.)

the implemented DT can perform state estimation in near real-time. Good performances were also achieved by leveraging the developed adapters that produce a continuous data flow without any interruptions.

In addition, Fig. 15(a) and (b) report the details of the calculation carried out on 01/09/2022 and 02/09/2022, respectively. The figure provides a comparison between measured and calculated voltage profiles which are referred to Bus 2 in Fig. 9. Fig. 15(b) shows an interesting behavior of the state estimation algorithm that was able to follow a rapid voltage drop of 8% around 13:00. During the other timestamps reported in Fig. 15(a) and (b), the normal behavior of the state estimation was required and a good agreement between measured and calculated values was found.

Finally, Figs. 16 and 17 are selected among the timestamps to show the difference between the two stopping criteria, i.e. minimum tolerance in absolute value on the average error (Fig. 16) and the maximum number of generations (Fig. 17).

Finally, some results on the IEEE 33-nodes test case are reported, based on 4 sets of 50 simulations. For each set of simulations, N_M is fixed. However, the group of monitored nodes is randomly defined for each simulation (i.e., 50 different configurations are evaluated). It is worth mentioning that power profiles are the same for all the simulations and were carried out assuming that the exact status of the network is known at the first timestamp (i.e., the state estimation overcame the start-up transient).

Results of the 200 simulations are averaged and reported in Table 8, which shows that the state estimation can still provide good performances on accuracy and execution time.

4.2. Flexibility calculator

This subsection presents the main performances of the flexibility calculator during DT near real-time operation. Fig. 18(a) shows the active power flow in the main feeder (line 1 in Fig. 9)

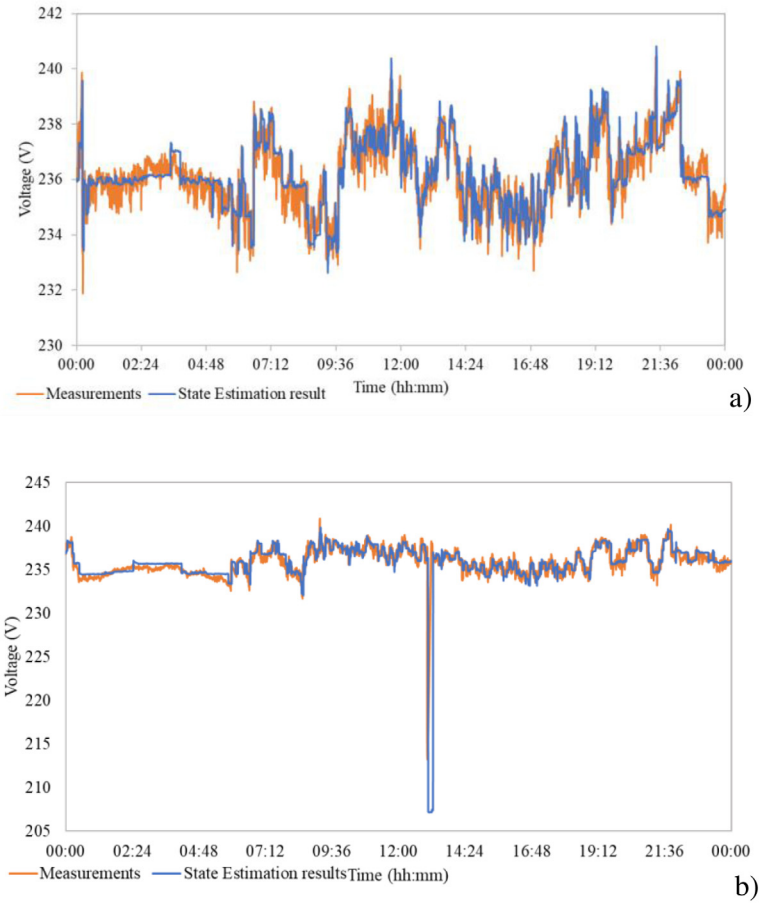

Fig. 15. Measured and calculated voltage profiles at bus 2 on (a) 01/09/2022 and (b) 02/09/2022.

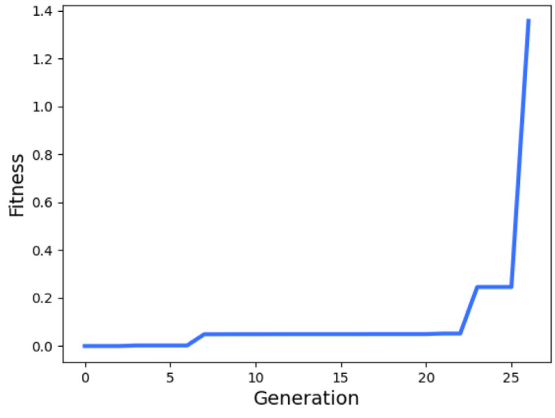

Fig. 16. Fitness evolution when GA in state estimation stops since minimum tolerance in absolute value on the average error is achieved.

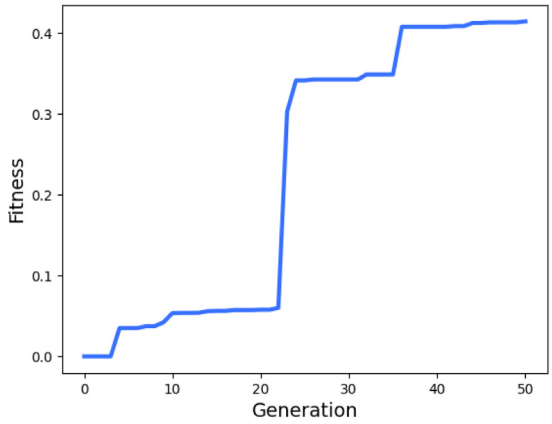

Fig. 17. Fitness evolution when GA in state estimation stops since the maximum number of generations is reached.

Table 8
Results of the state estimation applied on the test network.

N_M	Average time (s)	Average error (V)	Median time (s)	Median error (V)
25	0.0200	0.1612	0.0239	0.0223
20	0.0186	0.0736	0.0220	0.0235
15	0.0176	0.0688	0.0209	0.0276
10	0.0165	0.0561	0.0190	0.0307

with and without the use of flexible resources during a week in September 2022, considering actual consumption and generation data, post-processed by the state estimation. Fig. 18(b) and (c) show selected time windows of the power flow in Fig. 18(a), one day, and one hour, respectively. A recurring trend is evident: flexibility resources recharge between 9 a.m. and 12 p.m., when PV production is increasing and load demand is still limited, and discharge in the pre-evening hours to reduce peak power. As can be seen in detail in Fig. 18(c), the flexibility management system allows for avoiding some peaks by returning them to a value close

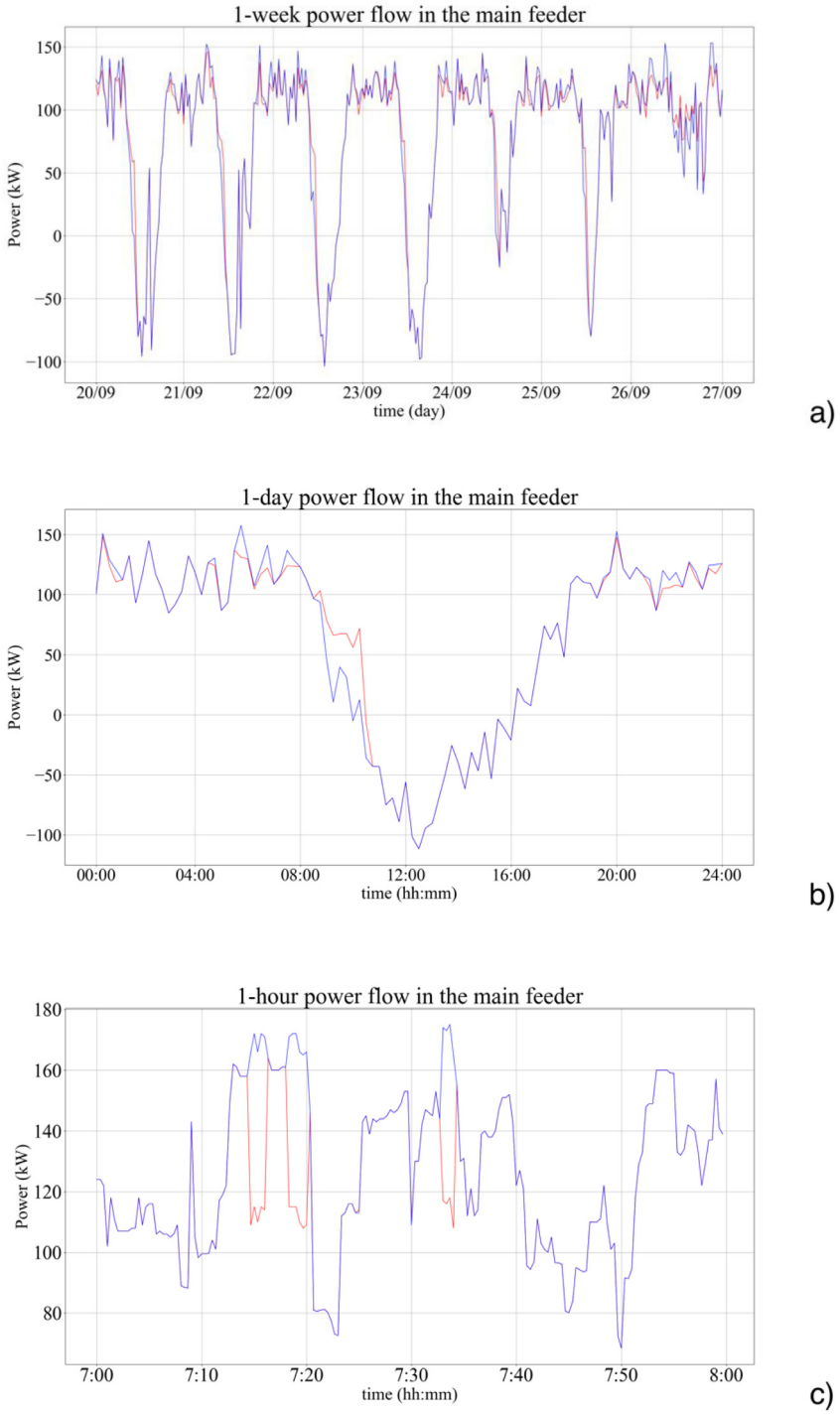

Fig. 18. Active power flow in the main feeder during (a) one week in September; (b) one day (22 of September); (c) one hour. Blue line: measurements; red line: power flow using flexibility resources . (For interpretation of the references to color in this figure legend, the reader is referred to the web version of this article.)

to the average, while for others peaks does not act with such effectiveness. The reason is that the system operates at thresholds with a non-linear response and that the flexibility resources once saturated can no longer deliver the services until they become available again.

Fig. 19 shows the available energy of the flexibility resources, namely three flexible loads connected to buses 8, 10, and 11 and two EESS connected to buses 9 and 14, during three days of the second half of September 2022. The use of flexible resources follows a similar trend for all storage objects, due to the unique storage controller governing all resources, albeit with different power and energy limitations. As Fig. 19 shows, resources are recharged in the middle hours of the day, when PV production is highest and the power flow in the main feeder is low or negative, and are discharged from late afternoon to morning.

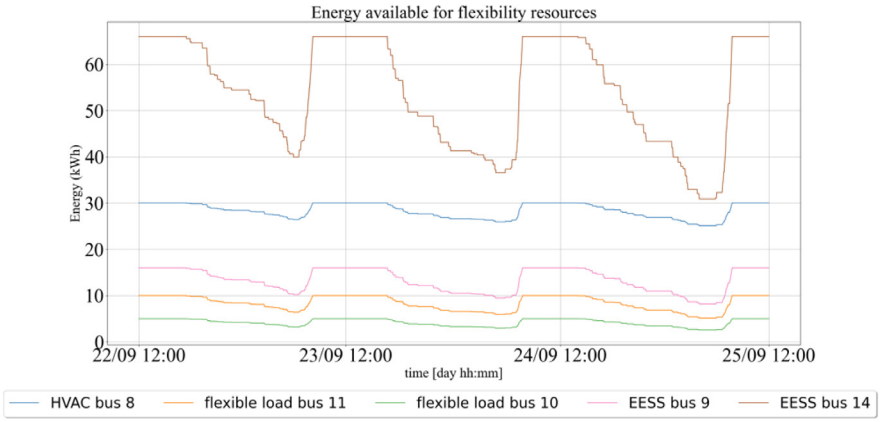

Fig. 19. Available energy from flexibility resources installed in the case study during three days in September.

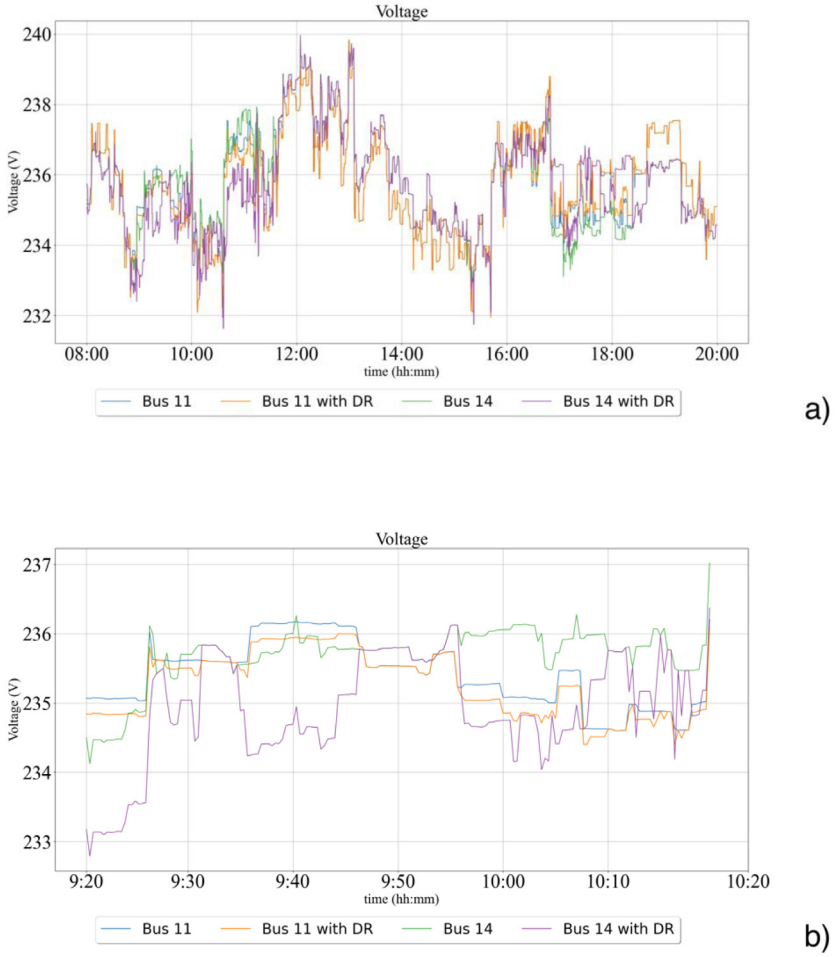

Fig. 20. Voltage profile of two buses on the 22 of September in (a) a 12-h time window and in (b) a one-hour time window with and without the use of flexibility services.

The use of flexibility does not significantly alter bus voltage profiles because the implemented algorithm does not optimize bus voltages but rather tries to increase the self-consumption of the network portion. Indeed, the average bus voltage values with and without flexibility are 236.124 V and 236.137 V respectively, with a standard deviation of 1.502 V and 1.516 V. Figs. 20(a) and 19(b) clarifies such aspect, clearly showing that only small voltage deviations occur in the network when flexibility is exploited.

As expected, the impact of flexibility resources on currents is larger than what happens for voltage. The reduction of the average current values on each line is about 4.57%, with a reduction in the standard deviation of 11.48%. Fig. 21(a) and (b) highlight this effect, allowing in this way the reduction of network losses and the reduction of thermal risks.

Lastly, Table 9 reports some aggregate results obtained after one month of DT operation. The SCR is increased from 88.42% up to 91.99% and reverse energy flows along the main feeder are reduced by 33.01%, with benefits for both LV users and DSO. The

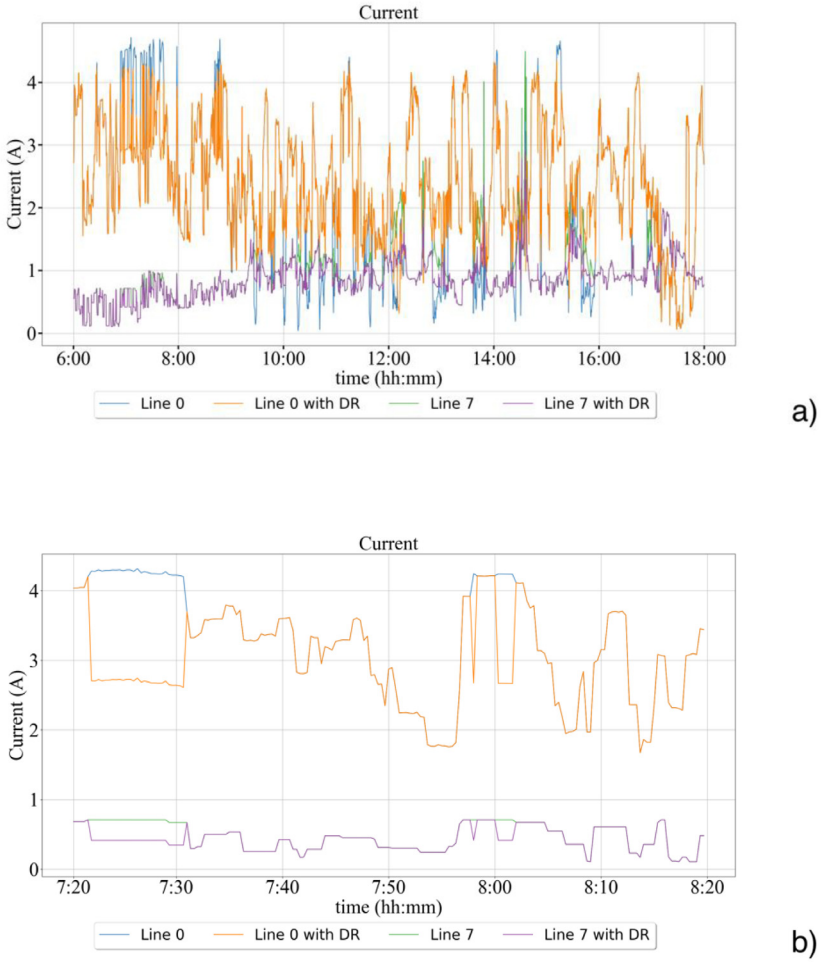

Fig. 21. Current profile of two lines on the 22 of September in (a) 12-h time-window and (b) a one-hour time-window with and without the use of flexibility services.

Table 9
Effect of DT operation on global indicators.

Parameter	Without DT	With DT
SCR (%)	88.42	91.99
Reverse energy flows (kWh/month)	2999	2022
Max power in main feeder (kW)	345	263
Min power in main feeder (kW)	−204	−148

peak of the power drawn from the distribution grid is reduced by 23.7%, while the peak from the distribution grid to the external network is reduced by 27.4% in the analyzed month.

5. Conclusion

This paper presents a DT development and its validation on a real DN. Although in many fields DT is widely considered an enabling technology for innovation, applications on electric power systems are still limited and unified approaches are lacking. This work takes advantage of the consolidated experience of DT architecture in other fields (i.e., smart manufacturing and building management) and exploits their achievements to develop a DT for the near real-time analysis of an active DN.

First, some modules were developed, notably data collection entity, state estimation, and flexibility calculator, and then have been integrated into a DT. The modules exploit open-source resources, aiming at integrating a variety of field devices as well as to couple of already developed modules that could provide different services. In this way, the DT is highly scalable and flexible. Based on the reference architecture, some modules are implemented in a real case study, involving a MV feeder where near real-time smart meters, renewable energy sources, and flexible loads are exploited for the DT evaluation. After one month of operation, it was reported that the developed DT had continuously operated, integrating all the field devices and the developed modules. The state estimation showed good accuracy in providing continuous service in a near real-time way; it increases operator awareness about the current status of the DN as well as it offers a consolidated dataset for the flexibility calculator or other modules. The flexibility calculator during one month of operation was able to provide set of requests in a near real-time way without any service interruptions. Results highlight the module's ability to increase the grid's SCR and limit power cable loading.

Finally, this article showed the validation of the DT when it is coupled with a real distribution network operating near real-time. During the operation, the DT has adequately performed so that its integration with a real network was achieved and validated.

In the upcoming work, the authors will improve the quality and the performances of the DT, focusing on specific aspects such as the difficulty of estimating the DN state in situations that deviate significantly from historical data and the use of different algorithms for the flexibility calculator to overcome problems due to resource saturation and system stability issues. Finally, the authors wish to deepen the definition of flexible resources, going into more detail on the constitutive models of each component

and validating the DT on a real infrastructure, evaluating to what extent the actual response of the components corresponds to the one predicted by the analytical model.

CRediT authorship contribution statement

T. Bragatto: Conceptualization, Methodology, Software, Formal analysis, Writing – original draft. **M.A. Bucarelli:** Conceptualization, Methodology, Software, Writing – original draft. **F. Carere:** Investigation, Data curation. **M. Cresta:** Resources. **F.M. Gatta:** Investigation. **A. Geri:** Conceptualization, Methodology, Supervision. **M. Maccioni:** Validation, Writing – review & editing. **M. Paulucci:** Resources. **P. Poursoltan:** Software, Data curation. **F. Santori:** Resources.

Declaration of competing interest

The authors declare that they have no known competing financial interests or personal relationships that could have appeared to influence the work reported in this paper.

Data availability

Some datasets will be available on request. Other dataset cannot be shared.

Acknowledgments

The publication was partially created with the co-financing of the European Union - FSEREACT-EU, PON Research and Innovation 2014-2020 DM1062 / 2021.

This work has been partially funded by the European Union's Horizon 2020 research and innovation programme under the I-NERGY project grant agreement No. 101016508.

References

[1] M. Grieves, J. Vickers, Digital twin: Mitigating unpredictable, undesirable emergent behavior in complex systems, in: Transdisciplinary Perspectives on Complex Systems: New Findings and Approaches, 2016, http://dx.doi.org/10.1007/978-3-319-38756-7_4.

[2] Y. Lu, C. Liu, K.I.K. Wang, H. Huang, X. Xu, Digital twin-driven smart manufacturing: Connotation, reference model, applications and research issues, Robot. Comput.-Integr. Manuf. 61 (2020) http://dx.doi.org/10.1016/j.rcim.2019.101837.

[3] Z. Liu, N. Meyendorf, N. Mrad, The role of data fusion in predictive maintenance using digital twin, in: AIP Conference Proceedings, 2018, p. 1949, http://dx.doi.org/10.1063/1.5031520.

[4] R.N. Bolton, et al., Customer experience challenges: bringing together digital, physical and social realms, J. Serv. Manage. 29 (5) (2018) http://dx.doi.org/10.1108/JOSM-04-2018-0113.

[5] M. Batty, Digital twins, Environ. Plan. B Urban Anal. City Sci. (2018).

[6] A. Fuller, Z. Fan, C. Day, C. Barlow, Digital twin: Enabling technologies, challenges and open research, IEEE Access 8 (2020) http://dx.doi.org/10.1109/ACCESS.2020.2998358.

[7] C. Cimino, E. Negri, L. Fumagalli, Review of digital twin applications in manufacturing, Comput. Ind. 113 (2019) http://dx.doi.org/10.1016/j.compind.2019.103130.

[8] M. Liu, S. Fang, H. Dong, C. Xu, Review of digital twin about concepts, technologies, and industrial applications, J. Manuf. Syst. 58 (2021) http://dx.doi.org/10.1016/j.jmsy.2020.06.017.

[9] E. O'Dwyer, I. Pan, R. Charlesworth, S. Butler, N. Shah, Integration of an energy management tool and digital twin for coordination and control of multi-vector smart energy systems, Sustain. Cities Soc. 62 (2020) http://dx.doi.org/10.1016/j.scs.2020.102412.

[10] J. Wang, L. Ye, R.X. Gao, C. Li, L. Zhang, Digital twin for rotating machinery fault diagnosis in smart manufacturing, Int. J. Prod. Res. 57 (12) (2019) http://dx.doi.org/10.1080/00207543.2018.1552032.

[11] F. Tao, M. Zhang, Y. Liu, A.Y.C. Nee, Digital twin driven prognostics and health management for complex equipment, CIRP Ann. 67 (1) (2018) http://dx.doi.org/10.1016/j.cirp.2018.04.055.

[12] N. Bazmohammadi, et al., Microgrid digital twins: Concepts, applications, and future trends, IEEE Access 10 (2022) http://dx.doi.org/10.1109/ACCESS.2021.3138990.

[13] B.R. Barricelli, E. Casiraghi, D. Fogli, A survey on digital twin: Definitions, characteristics, applications, and design implications, IEEE Access 7 (2019) http://dx.doi.org/10.1109/ACCESS.2019.2953499.

[14] J.-F. Uhlenkamp, J.B. Hauge, E. Broda, M. Lütjen, M. Freitag, K.-D. Thoben, Digital twins: A maturity model for their classification and evaluation, IEEE Access 10 (2022) 69605–69635, http://dx.doi.org/10.1109/ACCESS.2022.3186353.

[15] C. Antal, et al., Blockchain based decentralized local energy flexibility market, Energy Rep. 7 (2021) http://dx.doi.org/10.1016/j.egyr.2021.08.118.

[16] P. Koukaras, et al., A tri-layer optimization framework for day-ahead energy scheduling based on cost and discomfort minimization, Energies (Basel) 14 (12) (2021) http://dx.doi.org/10.3390/en14123599.

[17] Y. Peng, H. Wang, Application of digital twin concept in condition monitoring for DC-DC converter, in: 2019 IEEE Energy Conversion Congress and Exposition, ECCE 2019, 2019, http://dx.doi.org/10.1109/ECCE.2019.8912199.

[18] T. Barszcz, M. Zabaryłło, Concept of automated malfunction detection of large turbomachinery using machine learning on transient data, Diagnostyka 20 (1) (2019) http://dx.doi.org/10.29354/diag/100399.

[19] L.D. Gitelman, M. v. Kozhevnikov, D.D. Kaplin, Asset management in grid companies using integrated diagnostic devices, Int. J. Energy Prod. Manage. 4 (3) (2019) http://dx.doi.org/10.2495/EQ-V4-N3-230-243.

[20] Nandha Kumar Kandasamy, Sarad Venugopalan, Tin Kit Wong, Nicholas Junming Leu, An electric power digital twin for cyber security testing, research and education, Comput. Electr. Eng. 101 (2022).

[21] A. Saad, S. Faddel, T. Youssef, O.A. Mohammed, On the implementation of IoT-based digital twin for networked microgrids resiliency against cyber attacks, IEEE Trans. Smart Grid 11 (6) (2020) http://dx.doi.org/10.1109/TSG.2020.3000958.

[22] R. Darbali-Zamora, J. Johnson, A. Summers, C. Birk Jones, C. Hansen, C. Showalter, State estimation-based distributed energy resource optimization for distribution voltage regulation in telemetry-sparse environments using a real-time digital twin, Energies (Basel) 14 (3) (2021) http://dx.doi.org/10.3390/en14030774.

[23] J. Han, Q. Hong, Z. Feng, M. Syed, G. Burt, C. Booth, Design and implementation of a real-time hardware-in-the-loop platform for prototyping and testing digital twins of distributed energy resources, Energies (Basel) 15 (18) (2022) 6629, http://dx.doi.org/10.3390/en15186629.

[24] H.A. Park, G. Byeon, W. Son, H.C. Jo, J. Kim, S. Kim, Digital twin for operation of microgrid: Optimal scheduling in virtual space of digital twin, Energies (Basel) 13 (20) (2020) http://dx.doi.org/10.3390/en13205504.

[25] E. Ferko, A. Bucaioni, M. Behnam, Architecting digital twins, IEEE Access 10 (2022) 50335–50350, http://dx.doi.org/10.1109/ACCESS.2022.3172964.

[26] ISO 23247-2:2021 Automation systems and integration — Digital twin framework for manufacturing — Part 2: Reference architecture.

[27] R. Cloutier, G. Muller, D. Verma, R. Nilchiani, E. Hole, M. Bone, The concept of reference architectures, Syst. Eng. 13 (1) (2010) http://dx.doi.org/10.1002/sys.20129.

[28] K.M. Alam, A. el Saddik, C2PS: A digital twin architecture reference model for the cloud-based cyber–physical systems, IEEE Access 5 (2017) http://dx.doi.org/10.1109/ACCESS.2017.2657006.

[29] Y. Zheng, S. Yang, H. Cheng, An application framework of digital twin and its case study, J. Ambient Intell. Hum. Comput. 10 (3) (2019) http://dx.doi.org/10.1007/s12652-018-0911-3.

[30] R.C. Dugan, A. Ballanti, Opendss manual, Train. Mater. (March) (2016).

[31] D. Krishnamurthy, Opendssdirect.py. https://github.com/dss-extensions/OpenDSSDirect.py.

[32] A.J. Conejo, L. Baringo, Power System Operations, Springer International Publishing AG, Cham, Switzerland, 2018.

[33] S. Katoch, S.S. Chauhan, V. Kumar, A review on genetic algorithm: past, present, and future, Multimed. Tools Appl. 80 (2021) 8091–8126, http://dx.doi.org/10.1007/s11042-020-10139-6.

[34] Ahmed Fawzy Gad, PyGAD: An open-source python library for building the genetic algorithm and training machine learning algorithms pygad.readthedocs.io, 2020.

[35] M.Z. Degefa, I.B. Sperstad, H. Sæle, Comprehensive classifications and characterizations of power system flexibility resources, Electr. Power Syst. Res. 194 (2021) http://dx.doi.org/10.1016/j.epsr.2021.107022.

[36] S. Mohanty, et al., Demand side management of electric vehicles in smart grids: A survey on strategies, challenges, modelling, and optimization, Energy Rep. 8 (2022) 12466–12490, http://dx.doi.org/10.1016/j.egyr.2022.09.023.

[37] M. Rastegar, Impacts of residential energy management on reliability of distribution systems considering a customer satisfaction model, IEEE Trans. Power Syst. 33 (6) (2018) http://dx.doi.org/10.1109/TPWRS.2018.2825356.

[38] R. Sharifi, S.H. Fathi, V. Vahidinasab, A review on demand-side tools in electricity market, Renew. Sustain. Energy Rev. 72 (2017) http://dx.doi.org/10.1016/j.rser.2017.01.020.

[39] N.G. Paterakis, O. Erdinç, A.G. Bakirtzis, J.P.S. Catalão, Optimal household appliances scheduling under day-ahead pricing and load-shaping demand response strategies, IEEE Trans. Ind. Inform. 11 (6) (2015) http://dx.doi.org/10.1109/TII.2015.2438534.

[40] Bryony Parrish, Phil Heptonstall, Rob Gross, Benjamin K. Sovacool, A systematic review of motivations, enablers and barriers for consumer engagement with residential demand response, Energy Policy (ISSN: 0301-4215) 138 (2020) 111221, http://dx.doi.org/10.1016/j.enpol.2019.111221.

[41] G. Morales-España, R. Martínez-Gordón, J. Sijm, Classifying and modelling demand response in power systems, Energy 242 (2022) http://dx.doi.org/10.1016/j.energy.2021.122544.

[42] F. Carere, T. Bragatto, F. Santori, A distribution network during the 2020 COVID-19 pandemic, in: 12th AEIT International Annual Conference, AEIT 2020, 2020, http://dx.doi.org/10.23919/AEIT50178.2020.9241191.

[43] A. Geri, et al., Distributed generation monitoring: a cost-effective raspberry pi-based device, in: 2022 2nd International Conference on Innovative Research in Applied Science, Engineering and Technology, IRASET 2022, 2022, http://dx.doi.org/10.1109/IRASET52964.2022.9737768.

[44] I-NERGY Project Consortium. I-NERGY – Artificial Intelligence for Next Generation Energy. https://i-nergy.eu/.

[45] T. Bragatto, et al., Innovative tools for demand response strategies: A real-life experience, in: Proceedings - 2019 IEEE International Conference on Environment and Electrical Engineering and 2019 IEEE Industrial and Commercial Power Systems Europe, EEEIC/I and CPS Europe 2019, 2019, http://dx.doi.org/10.1109/EEEIC.2019.8783584.

[46] T. Bragatto, M. Cresta, V. Croce, M. Paulucci, F. Santori, D. Ziu, A real-life experience on 2nd life batteries services for distribution system operator, in: Proceedings - 2019 IEEE International Conference on Environment and Electrical Engineering and 2019 IEEE Industrial and Commercial Power Systems Europe, EEEIC/I and CPS Europe 2019, 2019, http://dx.doi.org/10.1109/EEEIC.2019.8783963.

[47] F. Carere, et al., Flexibility - enabling technologies using electric vehicles, in: Proceedings - 2020 IEEE International Conference on Environment and Electrical Engineering and 2020 IEEE Industrial and Commercial Power Systems Europe, EEEIC/ I and CPS Europe 2020, 2020, http://dx.doi.org/10.1109/EEEIC/ICPSEurope49358.2020.9160781.

[48] M. Sanduleac, M. Albu, J. Martins, M.D. Alacreu, C. Stanescu, Power quality assessment in LV networks using new smart meters design, in: Proceedings - 2015 9th International Conference on Compatibility and Power Electronics, CPE 2015, 2015, http://dx.doi.org/10.1109/CPE.2015.7231057.

[49] M.M. Albu, M. Sănduleac, C. Stănescu, Syncretic use of smart meters for power quality monitoring in emerging networks, IEEE Trans. Smart Grid 8 (1) (2017) http://dx.doi.org/10.1109/TSG.2016.2598547.

[50] M.E. Baran, F.F. Wu, Network reconfiguration in distribution systems for loss reduction and load balancing, IEEE Trans. Power Deliv. 4 (2) (1989) 1401–1407, http://dx.doi.org/10.1109/61.25627.

[51] A report prepared by the Reliability Test System Task Force of the Application of Probability Methods Subcommittee, IEEE reliability test system, IEEE Trans. Power Appar. Syst. PAS-98 (6) (1979) 2047–2054.